Nonlinear Behavior of IM7 Carbon Fibers in Compression Leads to Bending Nonlinearity of High-Strain Composites

Uba K Ubamanyu,* and Sergio Pellegrino†
California Institute of Technology, Pasadena, CA, 91125, USA.

This paper presents an experimental characterization of carbon fibers under compression and the influence of their nonlinear behavior on the bending nonlinearity of high-strain composites (HSC). The study is focused on HexTow IM7, a pan-based carbon fiber compressed under in-situ scanning electron microscopic (SEM) imaging. The sample preparation and experimental procedure of both single fiber direct compression tests and column bending tests of HSC samples are presented. Nonlinearity at the individual fiber level could not be observed due to the limitations of the load cell in the single fiber direct compression experiment. Using the column bending tests, a shift in the neutral axis due to the nonlinear compression behavior of fibers is observed.

I. Introduction

Fiber-reinforced polymer composites are engineered materials that consist of fibers embedded inside a polymeric matrix. Deployable structures made of high-strain composites (HSC) are of increasing interest due to their high stiffness-to-weight ratio, high packaging efficiency, and ability to deploy by the release of stored strain energy. Carbon fiber is one of the most common fiber constituents in high-strain composites used for space applications. Carbon fibers fall into two main categories based on their manufacturing methods: polyacrylonitrile (pan)-based and pitch-based. The nanostructure of carbon fibers is made with graphite layers.

Studies over the past decades have shown that carbon fiber-reinforced polymer composites have higher tensile strength compared to their compressive strength. Initial studies attributed this effect to fiber microbuckling based on elastic shear instabilities and initial misalignment [1–3]. Later on, nonlinear effects in the carbon fibers were identified from single fiber tests [4–7]. The hardening behavior of pan-based carbon fiber under tensile loading has been studied extensively. Several constitutive models were developed based on strain energy density [8], and considering the reorientation of the fibers' crystalline nanostructure [9] to capture the hardening nonlinearity. While many researchers have modeled the hardening behavior using a phenomenological approach, Northolt et al. [9] explained this effect in terms of the physical nanostructure of pan-based carbon fiber, observed by Barnet and Norr [10]. Pan-based carbon fibers consist of circumferential graphitic basal planes with a less oriented crystalline core. Reorientation of the misaligned basal planes due to increasing strain influences the shear modulus between the basal planes, and hence attributes to the nonlinearity of carbon fiber under tension. However, the nonlinearity of carbon fiber under compression has not been studied in depth. Recent experimental efforts [5, 6] have shed light on the range of nonlinearity of T800S and T300 carbon fibers using a single fiber direct compression test. Results from these studies show that the failure strain under compression (approximately 10%) is much larger than the tensile failure strain (2%), while the compression strength is almost half of the tensile strength. Furthermore, X-ray diffraction measurements of bent carbon fiber by Loidl et al [7] confirmed that the tensile and compression moduli are different and a shift in the neutral axis of bending was observed at the single fiber level. Schlothauer et al [11] showed that Northolt's model can be extended to the compression region while the original model had only been developed for tension. They successfully demonstrated the nonlinear material modeling incorporating the Northolt model spanning tension and compression region, for uni-directional thin-ply T800S carbon fiber reinforced composites. As a result of the fiber nonlinearity, thin composite samples exhibit a shift in the neutral axis under high curvature [11].

The goal of this paper is to characterize the compression behavior of pan-based HexTow IM7 carbon fibers and determine how the nonlinearity of fibers influence the bending nonlinearity of high-strain composites. Our current study is focused on individual HexTow IM7 carbon fibers. Section II explains the sample preparation and the in-situ SEM experimental procedure to characterize the behavior of individual carbon fibers under compression and presents a

*Graduate Student, Graduate Aerospace Laboratories, 1200 E California Blvd, MC 105-50, Pasadena.
†Joyce and Kent Kresa Professor of Aerospace and Civil Engineering, Graduate Aerospace Laboratories, 1200 E California Blvd, MC 105-50, Pasadena. AIAA Fellow.

compressive stress-strain response showing the nonlinearity of the fibers. Section III presents the details of the column bending test of HSC samples and the nonlinearity observed under bending and the resulting shift in the neutral axis. Section IV, concludes the paper and outlines potential future work.

II. Compression Nonlinearity of the Carbon Fiber

Despite many attempts, measurement of the compressive stress-strain response of an individual fiber is still extremely difficult. The lack of accurate and repeatable standardized test methods is a key challenge. The diameter of fibers, in the range 5-10 μm, is the major obstacle and makes the sample preparation time-consuming. The fiber needs to be properly aligned and clamped in order to avoid eccentric loading, which would result in buckling instead of pure compression. Due to the microscopic nature of the sample, the force and the displacement measurements are extremely small, hence, precise and accurate measurement devices are key to such an experiment. Several direct and indirect methods have been utilized to measure the compression modulus and strength of individual fibers. The elastica loop test [12], the beam bending test [13], the single fiber composite test [14], the tensile recoil test [15], and the direct compression test [5, 6, 16] with custom-made loading devices are some notable examples. These test methods either involve indirect measurements of compression behavior and/or use custom-made devices for measurements. Furthermore, Macturk et al [17] noted that the compression strengths obtained from different methods are not consistent. Past experimental observations clearly show that the compression behavior depends on the type of fiber and its manufacturing parameters such as fiber precursor, processing temperature, and the nanostructure [7, 13, 17]. To avoid the need for highly specialized, custom test equipment, for our study we decided to use a commercially available nanoindenter inside a scanning electron microscope (SEM).

To avoid buckling, the length of the fiber needs to be shorter than the critical buckling length, l_c. The critical buckling length was calculated from the Euler buckling equation, $P_{cr} = \frac{\pi^2 EI}{4l^2}$. Assuming the critical stress to be equal to tensile failure strength, σ_f, the tensile modulus reported in the Toray datasheet was used to estimate the critical buckling length, l_c:

$$l_c = \frac{\pi d}{8}\sqrt{\frac{E}{\sigma_f}} \tag{1}$$

Based on the material properties in Table 1, the length of IM7 fiber should be less than l_c = 14.4 μm to avoid buckling. In this study, a free length of 10 μm was considered. However, the compression modulus is known to be lower than the tensile modulus in high-strain regimes therefore, the calculated critical length to prevent buckling is only a preliminary estimate and needs to be verified later using the results from the experiments.

Table 1 Material datasheet values of IM7 fibers provided by the manufacturer [18]

Parameter	Value
Fiber diameter, d	5.2 μm
Tensile modulus, E	276 GPa
Tensile strength, σ_f	5688 MPa
Tensile failure strain, ϵ_f	1.9%

A. Sample Preparation

A polyacrylonitrile (pan)-based carbon fiber, HexTow IM7 with 12K filament count tow manufactured by Hexcel was chosen for this study. HexTow IM7 is a continuous, high-performance, and intermediate modulus fiber.

Individual fibers are separated and a small weight made of lead (sphere of 1 mm diameter) was attached at one end and hung vertically in a custom-made linear stage. Then the fiber was lowered into a 2 mm hole drilled on an aluminum SEM stud as shown in Fig. 1. Then epoxy resin (Loctite EA E-120HP) was applied using a needle and cured for 24 hours at room temperature. A minimum length of 1 mm of fiber was submerged into the epoxy resin. The overhanging fiber was cut by Ga+ focused ion beam using FEI DualBeam VERSA SEM. A beam with 30kV and 1nA was used for

the first pass and polished with 100pA current. The free length of the fiber was approximately 10 μm. The length of fiber embedded in the epoxy is much longer than the free length. An SEM image of a prepared sample is shown in Fig. 2

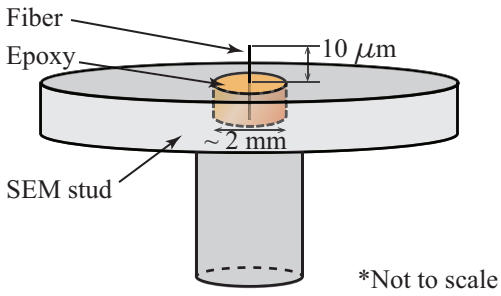

Fig. 1 Schematic (not drawn to scale) of a prepared sample.

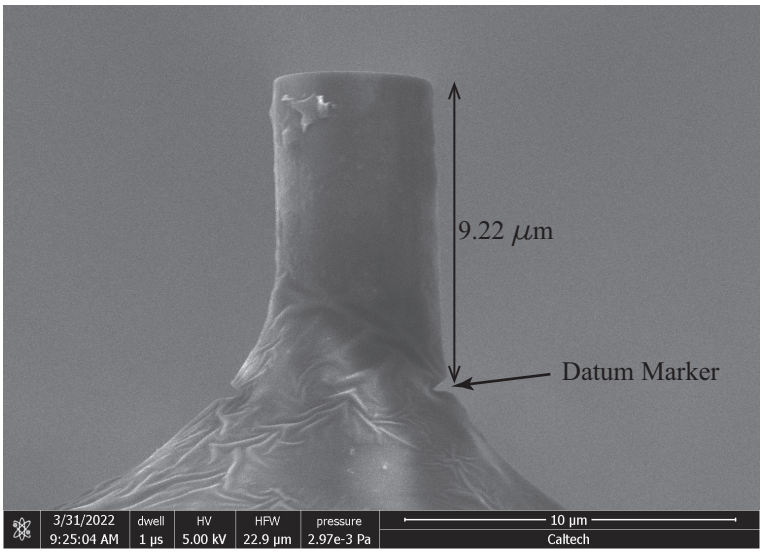

Fig. 2 SEM image of the prepared sample.

B. Direct Compression Test

The prepared fiber samples were compressed axially using a 170 μm diameter cylindrical nanoindenter (InSEM, Nanomechanics, Inc.) installed in a SEM (FEI Quanta 200F) to enable in-situ imaging. The samples were first loaded up to 20 mN and then unloaded before being loaded up to 49 mN (the load capacity of the nanoindenter load cell was 50 mN) and then unloaded, at a loading rate of 10 nm/s for both loading and unloading. The measured load was divided by the circular cross-sectional area of the fiber to calculate the mean compressive stress in the fiber and the strain was calculated by the change in length measured directly from the in-situ SEM images, see Fig.3. A marker was made closer to the end of the fiber using the focused ion beam as a datum point for the length measurements. Furthermore, the test results were discarded for the tests where the fiber columns underwent bending in addition to compression.

C. Results

A typical compressive stress-strain curve obtained from a direct compression test is shown in Fig. 4. The compression behavior is fairly linear in the low-strain region. The initial softening is ignored, assuming it was due to initial compliance of the indenter assembly. The nonlinear behavior of the compressive stress-strain response could not be observed during the test due to the limitations of our equipment. The capacity of the nanoindenter load cell is lower than the failure load of the carbon fiber. Hence, the test was interrupted before the final failure of the fiber and our measurements were

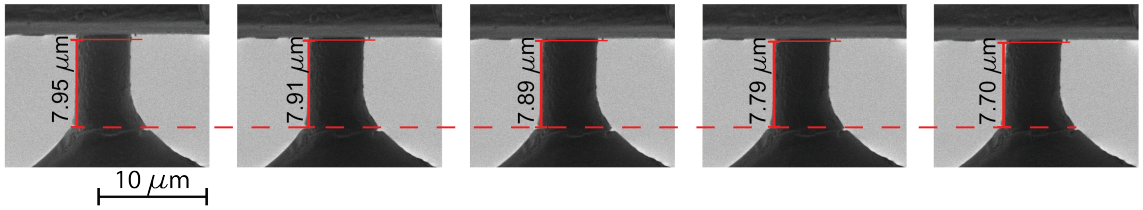

Fig. 3 Subset of the SEM image sequence used for length measurements, to calculate the compressive strain.

limited to lower strain region. However, the results we got for IM7 fibers closely match the linear regime of the T800 fibers reported in [5], but he nonlinearity is evident in the high-strain region for the T800 fibers. In order to characterize the nonlinearity of the IM7 fibers, the test needs to be repeated using a load cell with a high capacity.

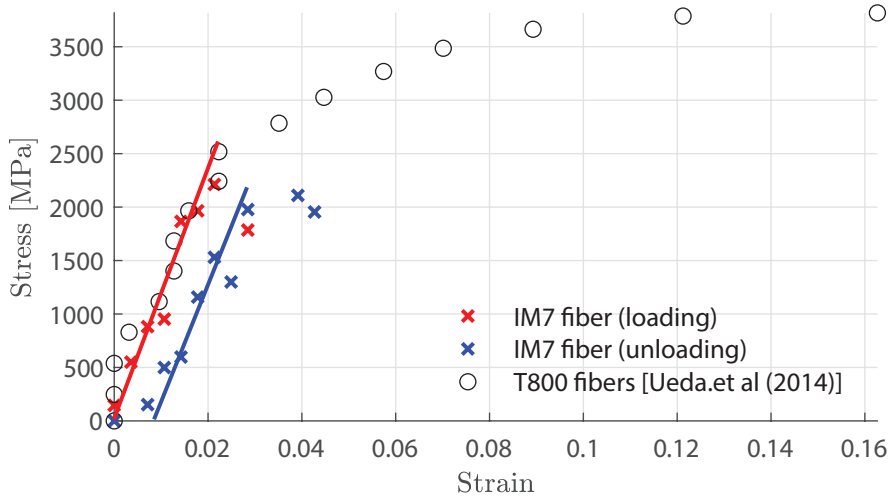

Fig. 4 Compression behavior of IM7 fibers during loading and unloading.

The compression modulus of carbon fiber can be calculated as a function of compressive strain from the above results and even extend the model using the T800 fiber response. One can model this behavior using the Northolt model [9] as demonstrated in [11] to simulate the material response of HSC structures. However, this is beyond the scope of this paper.

An important consideration for this test method is determining the free length of the sample. Two competing effects need to be taken into account. First is that the sample needs to be shorter than the critical buckling length to prevent buckling and second is that the sample needs to be longer than the decay length to avoid non-uniform stresses due to end effects, known as Saint-Venant's principle. The critical buckling length is estimated as ~14 μm using Eq. 1 considering the tensile modulus of the carbon fiber as explained in Section II. Note that the estimated critical buckling length using the tensile modulus is likely to be an overestimation of the actual buckling length because the compression modulus decreases with strain. Horgan[19] showed that for a transversely isotropic cylindrical rod, the decay length based on the Saint-Venant principle is $r\sqrt{\frac{E_l}{E_t}}$, where r is the radius of the cylinder, E_l and E_t are the elastic moduli in the longitudinal and transverse direction. However, it is difficult to calculate the decay length for carbon fibers precisely because the transverse modulus is unknown. As a result, the minimum length of carbon fiber to avoid end effects is estimated to be 23.3 μm, assuming $\frac{E_l}{E_t}$ is 20. These constraints must be taken into account when interpreting the results of tests on carbon fibers with a diameter of 5.2 μm. Therefore, the test results could be unreliable as the free length of a fiber with a diameter of 5.2 μm needs to be shorter than ~14 μm to avoid buckling and longer than ~23 μm to avoid end effects. Hence, it would be beneficial to carry out these tests for the different free lengths of fibers to experimentally validate the influence of end effects and the combined compression and bending deformations.

III. Bending Nonlinearity of the HSC Samples

Ultra-thin high-strain composite samples subjected to large bending deformations can sustain significantly higher strains compared to uniaxial deformations. The new generation deployable structures have relied on tighter packaging and coiling which results in higher curvatures and strains. The bending nonlinearity of HSC become relevant under high-curvature and high-strain region and is not studied well. This section explains the test procedure to estimate the bending nonlinearity of HSC made of IM7 carbon fibers with PMT-F7G epoxy and the shift in the neutral axis of bending using a column bending test [20].

A. Sample Preparation

The samples were manufactured from 145 gsm uni-directional carbon fiber (UDCF) prepregs of IM7-12K carbon fibers with PMT-F7G epoxy resin. Laminates consisting of 1-ply, 2-ply, and 4-ply were prepared and cured in an autoclave, with vacuum bagging at 350 °F. The manufactured plates were cut using a box cutter into 20 mm wide, 100 mm long samples, and the edges of the samples were polished using fine grit sandpaper to remove any defects that occurred during the cutting process. The thickness and the width of the samples were measured as, {125±4 μm, 20.01±0.22 mm}, {255±4 μm, 19.95±0.25 mm}, and {459±12 μm, 19.80±0.21 mm} for 1-ply, 2-ply, and 4-ply samples respectively.

B. Column Bending Tests

The standard test methods, such as the three-point bending test and four-point bending test, are only capable of imposing small deformations, hence most suited to characterize the linear behavior of HSC samples. The column bending test (CBT) method described in [20] is capable of imposing large bending deformations. A schematic of CBT is shown in Fig.5. The sample is clamped with an initial eccentricity, l_1 (= 2 mm), from the axis of rotation, and a compressive load is applied on two rotating rigid arms. The eccentricity of the load results in bending the composite sample.

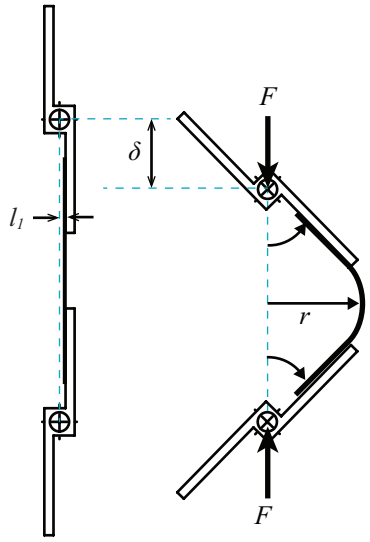

Fig. 5 Schematic of column bending test setup.

Samples were tested using custom-made CBT fixtures on an Instron 5569 mechanical testing machine equipped with a 500 N load cell as shown in Fig. 6. Displacement-controlled compression loading was applied at 10 mm/s. At least five samples from each category were tested.

The full-field displacements, strains, and curvatures were directly measured using a non-contact, 3D Digital Image Correlation (DIC) system from Correlated Solutions. Pairs of stereo-mounted digital cameras (Point-Grey Grasshopper3, 5 MP, Mono) at both the front and back of the test sample was used to image tensile and compression surface. The cameras were equipped with 35 mm focal length (Schneider Kreuznach Xenoplan) lenses and images were acquired using the VIC-Snap8 software at 500 ms. Both stereo DIC systems and the Instron were controlled using a NI-DAQ interface to start the testing and synchronize the measurements. Samples were sprayed with white spray paint to create a

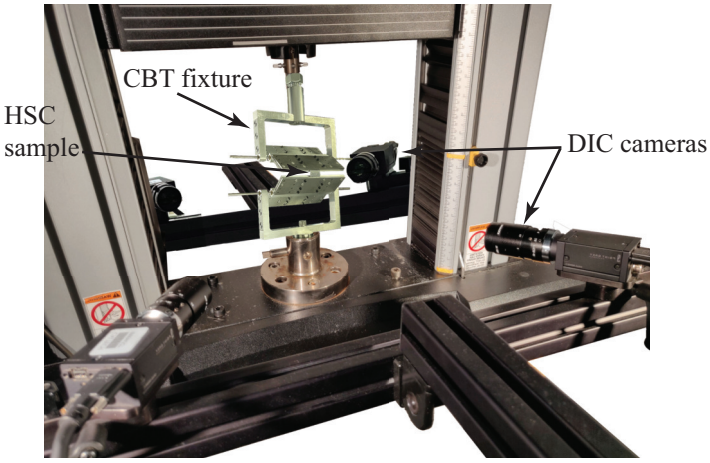

Fig. 6 Experimental setup for the CBT with digital image correlation measurements.

random pattern with speckle size between 5-10 pixels in order to avoid aliasing. Two white LED light arrays (WS3-K from REL Inc.) were used with white diffusers to scatter the light and avoid reflections while providing adequate lighting to keep the exposure time of the cameras around 20 ms. VIC3D (Correlated Solutions, v.7) software was used to triangulate each point on the surface using the pair of stereo images. The calibration was performed by capturing images by tilting, rotating, and translating a standard target (14 × 10 dots, spacing 3 mm) throughout the entire field of view. The DIC systems at the front and back were calibrated separately. The full-field displacement field was measured using a correlation algorithm utilizing Gaussian weights, optimized 8-tap spline interpolation, and zero-normalized square difference minimization function to ensure high sub-pixel accuracy and to compensate for the change in the lighting (brightness and contrast) during the test. A subset of 31 × 31 pixels and a step size of 7 pixels was chosen to achieve enough spatial resolution while maintaining low noise. A filter size of 15 pixels was used to calculate the strains and curvatures.

The bending moment on the sample was calculated as the product of the force recorded from the Instron load cell and the lever arm, r, shown in Fig.5. The lever arm was calculated as the sum of the initial offset l_1 (= 2 mm) and the maximum out-of-plane deformation of the sample which was measured using DIC. The curvature was calculated from the curvatures (κ_T, κ_C) measured at the center of the sample tensile and compression surfaces. Assuming Kirchhoff-Love plate theory, the curvature on the tensile surface is, $\kappa_T = 1/(r_c + t)$, and the curvature of the compression surface is, $\kappa_C = 1/r_c$ (see Fig.7). Therefore, the mid-surface curvature, κ is calculated from;

$$\kappa = \frac{2\kappa_C \kappa_T}{\kappa_C + \kappa_T} \tag{2}$$

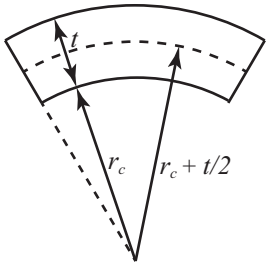

Fig. 7 Sketch of bent sample cross-section. The mid-surface is shown the dashed.

Note that all the quantities used for moment-curvature response were measured directly using DIC, as opposed to using the kinematic equations presented in [20]. These kinematic relations are based on the uniform curvature assumption and are sensitive to the accuracy of the free length. In addition to that, we observed that the error in curvature estimates increases with smaller free lengths as the end-effects become significant. A moment-curvature response is

shown in Fig.8. Note that not all of the samples were tested until failure due to the CBT fixtures coming into contact before the failure of the samples.

As expected the bending stiffness of the samples increases with the number of plies (see Fig. 8). To compare, the moment resultant was normalized by the thickness cubed and plotted against the curvature in Fig.9. This result demonstrates that all the experiments are repeatable and consistent as all the responses follow a similar trend. The bending nonlinearity is less pronounced in the global moment-curvature response of the samples. However, the nonlinear behavior of the fibers in compression becomes apparent when comparing the surface strain measurements on both compression and tension surfaces of the samples, shown in Fig.10.

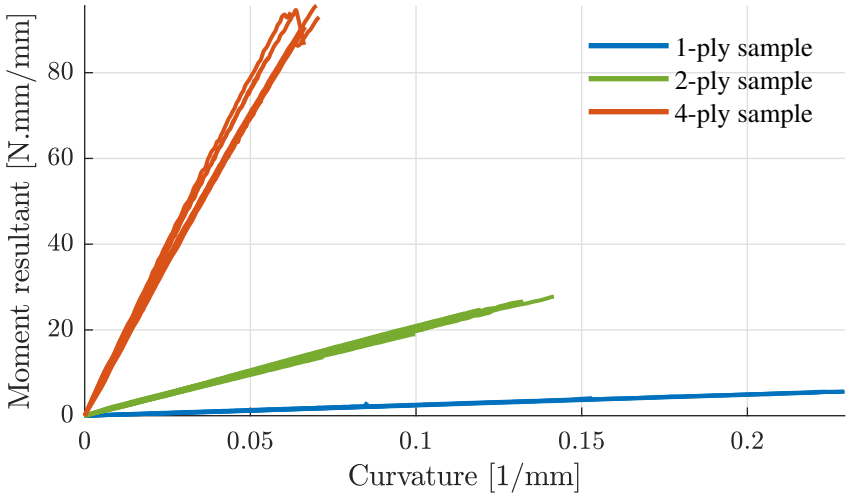

Fig. 8 Moment - curvature response of HSC samples.

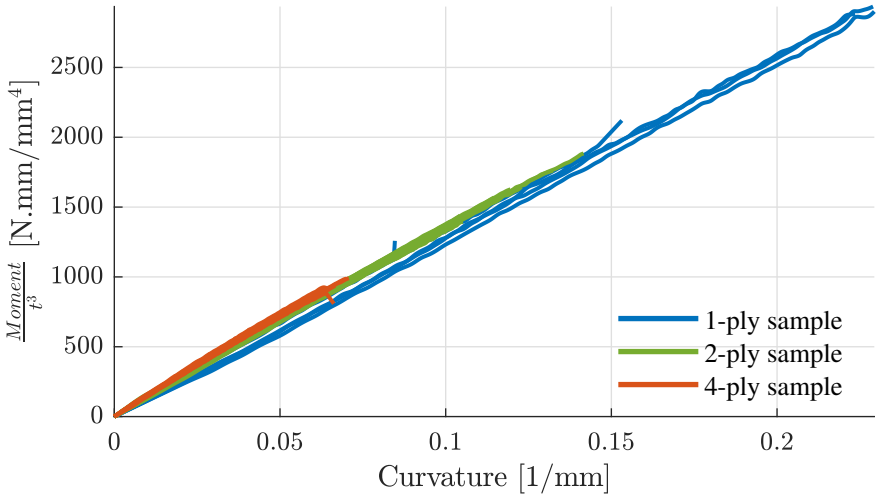

Fig. 9 Normalized moment - curvature response of HSC samples follows a single trend.

In a linear bending scenario, the two strains would be equal in magnitude (indicating that the neutral axis is fixed), but all samples show an increasing compressive surface strain. The compressive strain is ~25% higher than the tensile strain under high curvature. This behavior suggests that the neutral axis is shifting towards the tensile surface with increasing curvature.

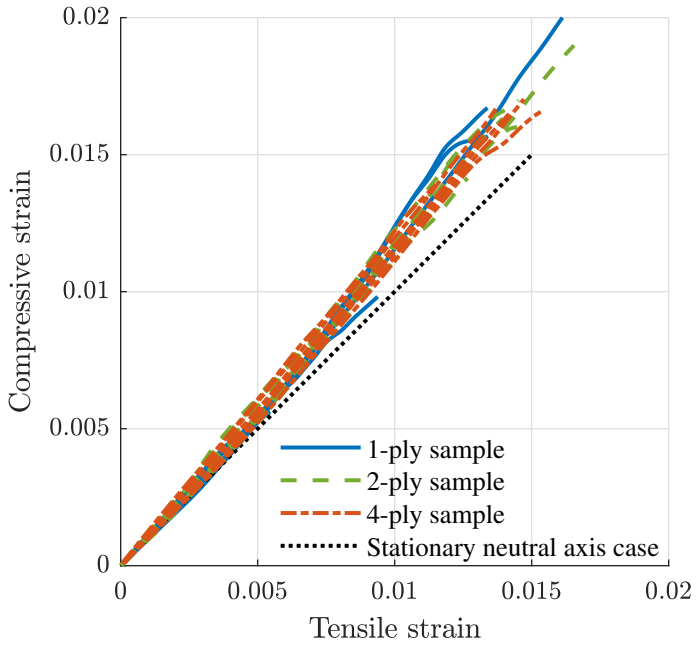

Fig. 10 Surface strains of HSC samples under bending.

C. Shift in Neutral axis

The measured surface strains indicate a shift of the neutral axis with increasing curvature. The shift is calculated using the linear through-thickness strain assumption, as shown in Fig. 11. The shift in the neutral axis, δ_{NA}, is given by,

$$\delta_{NA} = \frac{t}{2}\left(\frac{\epsilon_C - \epsilon_T}{\epsilon_C + \epsilon_T}\right) \tag{3}$$

where t is the laminate thickness, ϵ_C and ϵ_T are the measured longitudinal surface strains on the tension and compression surfaces respectively.

The shifts in the neutral axis with increasing curvature for different test samples were calculated and the mean and standard deviation were plotted for the samples with different thicknesses. They have been plotted in Fig. 12. The relative noise in the strain measurements is high in the low-strain region, hence, the low-curvature region has a larger standard deviation compared to the high-curvature region. An increasing shift in the neutral axis towards tension surface is clear from this result.

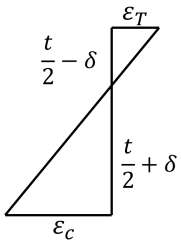

Fig. 11 Strain variation along the thickness.

IV. Conclusions

Our goal was to study the nonlinearity of HexTow IM7 carbon fibers under compression and its influence on the bending nonlinearity of laminates made from these fibers. In this paper, an experimental approach based on [5, 6] for a direct compression test of individual carbon fiber commonly used in high-strain composites has been described. We used

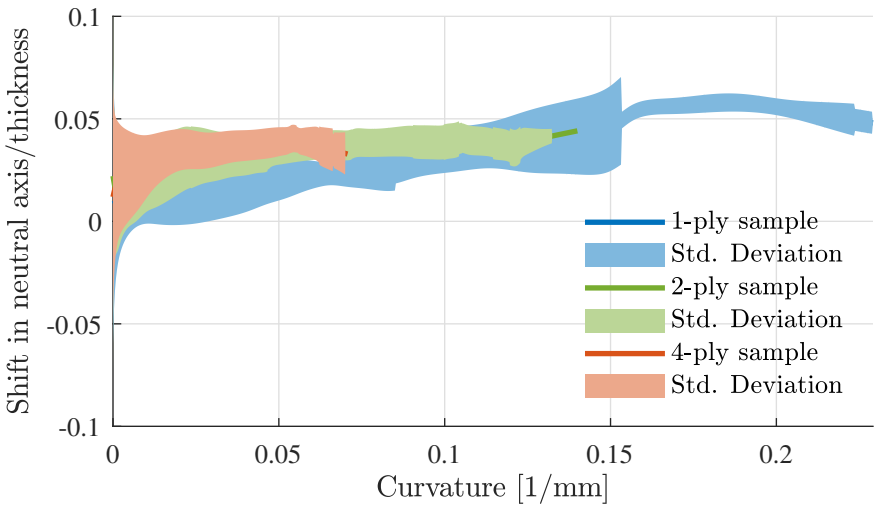

Fig. 12 Neutral axis shift in HSC samples calculated using Eq.(3).

a commercially available nanoindenter inside a scanning electron microscope for the direct compression test to avoid the need for highly specialized, custom test equipment. However, due to the inadequate capacity of the nanoindenter load cell, we could not achieve high strains where we expect to observe the nonlinearity of the fibers. Furthermore, it is important to note that the free length of the test fiber needs to be shorter than the critical buckling length (~14 μm) and longer than the decay length (~23 μm) to avoid end effects[19]. Therefore, despite the many advantages such as direct measurements of strain and stress, the result obtained from this method has its limitations. Hence, it would be beneficial to carry out these tests for the different free lengths of fibers to experimentally validate the influence of end effects and the combined compression and bending deformations.

The presented test results show the bending-nonlinearity of the HSC samples and a shift in the neutral axis of bending. The compressive strain measurements are ~25% higher than the tensile strains. The insights learned about the nonlinearity in the high-strain regime can be used for a better understanding of how design choices such as type of fiber-matrix combination, and laminate architecture affect the behavior of high-strain composite structures.

Acknowledgments

The authors acknowledge financial support from the Space Solar Power Project at Caltech. The authors are grateful for the help of Rebecca Gallivan, Widianto Moestopo, Thomas Tran, and Wenxin Zhang with single fiber direct compression experiments, and Professor Julia Greer for providing access to her experimental facilities and Alexander Wen for helpful discussions and suggestions. Test materials for this study were provided by Patz Materials & Technology.

References

[1] Rosen, B. W., "Mechanics of composite strengthening." 1965.

[2] Argon, A., "Fracture of Composites," *Treatise on Materials Science & Technology*, Vol. 1, Elsevier, 1972, pp. 79–114.

[3] Budiansky, B., "Micromechanics," *Computers & Structures*, Vol. 16, No. 1-4, 1983, pp. 3–12.

[4] Oliveira, L., Hitchcock, D., Behlow, H., Podila, R., Skove, M., Serkiz, S., and Rao, A., "Second-and third-order elastic constants of filaments of HexTow® IM7 carbon fiber," *Journal of materials engineering and performance*, Vol. 23, No. 3, 2014, pp. 685–692.

[5] Ueda, M., Saito, W., Imahori, R., Kanazawa, D., and Jeong, T.-K., "Longitudinal direct compression test of a single carbon fiber in a scanning electron microscope," *Composites Part A: Applied Science and Manufacturing*, Vol. 67, 2014, pp. 96–101.

[6] Ueda, M., and Akiyama, M., "Compression test of a single carbon fiber in a scanning electron microscope and its evaluation via finite element analysis," *Advanced Composite Materials*, Vol. 28, No. 1, 2019, pp. 57–71.

[7] Loidl, D., Paris, O., Burghammer, M., Riekel, C., and Peterlik, H., "Direct observation of nanocrystallite buckling in carbon fibers under bending load," *Physical review letters*, Vol. 95, No. 22, 2005, p. 225501.

[8] Ishikawa, T., Matsushima, M., and Hayashi, Y., "Hardening non-linear behaviour in longitudinal tension of unidirectional carbon composites," *Journal of materials science*, Vol. 20, No. 11, 1985, pp. 4075–4083.

[9] Northolt, M., Veldhuizen, L., and Jansen, H., "Tensile deformation of carbon fibers and the relationship with the modulus for shear between the basal planes," *Carbon*, Vol. 29, No. 8, 1991, pp. 1267–1279.

[10] Barnet, F. R., and Norr, M. K., "A three-dimensional structural model for a high modulus pan-based carbon fibre," *Composites*, Vol. 7, No. 2, 1976, pp. 93–99.

[11] Schlothauer, A., Pappas, G. A., and Ermanni, P., "Material response and failure of highly deformable carbon fiber composite shells," *Composites Science and Technology*, Vol. 199, 2020, p. 108378.

[12] Sinclair, D. A., "A Bending Method for Measurement of the Tensile Strength and Young's Modulus of Glass Fibers," *Journal of Applied Physics*, Vol. 21, 1950, pp. 380–386.

[13] DeTeresa, S. J., "The axial compressive strength of high performance polymer fibers," Tech. rep., Air Force Wright Aeronautical Labs Wright-Patterson AFB OH, 1985.

[14] Hawthorne, H., and Teghtsoonian, E., "Axial compression fracture in carbon fibres," *Journal of Materials Science*, Vol. 10, No. 1, 1975, pp. 41–51.

[15] Allen, S. R., "Tensile recoil measurement of compressive strength for polymeric high performance fibres," *Journal of materials science*, Vol. 22, No. 3, 1987, pp. 853–859.

[16] Oya, N., and Johnson, D. J., "Longitudinal compressive behaviour and microstructure of PAN-based carbon fibres," *Carbon*, Vol. 39, No. 5, 2001, pp. 635–645.

[17] Macturk, K., Eby, R., and Adams, W., "Characterization of compressive properties of high-performance polymer fibres with a new microcompression apparatus," *Polymer*, Vol. 32, No. 10, 1991, pp. 1782–1787.

[18] HexTow, "Carbon fiber product data sheet," *Hexcel Composites*, 2020.

[19] Horgan, C. O., "The axisymmetric end problem for transversely isotropic circular cylinders," *International journal of solids and structures*, Vol. 10, No. 8, 1974, pp. 837–852.

[20] Fernandez, J. M., and Murphey, T. W., "A Simple Test Method for Large Deformation Bending of Thin High Strain Composite Flexures," *2018 AIAA Spacecraft Structures Conference*, 2018, p. 0942.